Centrality dependence of thermal parameters deduced from hadron multiplicities in Au+Au collisions at $\sqrt{s_{NN}} = 130\,\text{GeV}$

J. Cleymans,[1] B. Kämpfer,[2] M. Kaneta,[3] S. Wheaton,[1] and N. Xu[4]
[1]*UCT-CERN Research Centre, Department of Physics, University of Cape Town, Rondebosch 7701, Cape Town, South Africa*
[2]*Institut für Kern- und Hadronenphysik, Forschungszentrum Rossendorf, PF 510119, D-01314 Dresden, Germany*
[3]*RIKEN BNL Research Center, Brookhaven National Laboratory, Upton, New York 11973*
[4]*Lawrence Berkeley National Laboratory, Berkeley, California 94720*
(Received 9 September 2004; published 5 May 2005)

We analyze the centrality dependence of thermal parameters deduced from hadron multiplicities in Au+Au collisions at $\sqrt{s_{NN}} = 130\,\text{GeV}$. Although the chemical freeze-out temperature and chemical potentials are found to be roughly centrality independent, the strangeness saturation factor γ_S increases with participant number toward unity, supporting the assumption of equilibrium freeze-out conditions in central collisions.

DOI: 10.1103/PhysRevC.71.054901 PACS number(s): 24.10.Pa, 25.75.Dw, 12.38.Mh

I. INTRODUCTION

Statistical-thermal models (cf. [1] for recent surveys and references therein) have enjoyed remarkable success in describing hadron multiplicities observed in both heavy-ion and elementary collisions over a wide range of energies [2–6]. The final state multiplicities are reproduced in these models with very few parameters. The prominent ones are the chemical freeze-out temperature T and baryon chemical potential μ_B. There are further chemical potentials to be considered below. A compilation of the freeze-out parameters over the accessible range of energies reveals a continuous curve in the $T - \mu_B$ plane that may be characterized by an energy per hadron of the order of 1 GeV [4]. Although the occurrence of such a universal freeze-out curve is interesting in itself and is useful for extrapolations and interpolations as well, its particular meaning could be the approximate coincidence with the confinement border line, at least at high energies, as conjectured in Ref. [7].

We do not touch here on the disputed question as to why also the multiplicities of the rare multistrange hadrons seem to obey chemical equilibrium (see [8]). Instead, we focus on one possible indicator of incomplete equilibrium, the strangeness saturation factor γ_s. This factor has been introduced [9] to account for an apparent undersaturation of strange hadrons. Various previous analyses [10] considered such a factor as necessary to accomplish a satisfactory description of data. For energies at Super Proton Synchrotron, $\sqrt{s_{NN}} = 6$–$20\,\text{GeV}$, it has been shown [11] that γ_s grows with increasing beam energy and centrality. First attempts [12], based on very restricted data sets, find also at the Relativistic Heavy Ion Collider (RHIC) energies a preliminary indication of rising γ_s with increasing centrality. It is the subject of this article to investigate in detail the dependence of the thermal parameters including γ_s on the centrality in collisions of Au+Au at $\sqrt{s_{NN}} = 130\,\text{GeV}$. By now there is a sufficiently large basis of published data at this energy to allow a thorough analysis.

Our article is organized as follows. In Sec. II we recall the formulation of our employed statistical-thermal model. The analyzed data are listed in Sec. III. Our fit procedures are described in Sec. IV and results are presented in Sec. V. The summary and conclusions can be found in Sec. VI.

II. STATISTICAL-THERMAL MODEL

For suitably large systems at RHIC collider energies, hadron multiplicities are analyzed by employing the grand-canonical partition function $\mathcal{Z}(V, T, \mu_i) = \text{Tr}[\exp\{-(\hat{H} - \sum_i \mu_i Q_i)/T\}]$, where $\hat{H}$ is the statistical operator of the system, T denotes the temperature, and μ_i and Q_i are respectively the chemical potentials and corresponding conserved charges in the system. To be specific, we use here the baryon charge (corresponding to μ_B) and the strangeness charge (corresponding to μ_S) as unconstrained quantities. [There are other possible chemical potentials (e.g., μ_Q as electric charge potential). However, we put $\mu_Q = 0$ with the reasoning explained below.]

The primordial particle numbers are accordingly,

$$N_i^{\text{prim}} = V g_i \int \frac{d^3p}{(2\pi)^3}\, dm_i \left[\gamma_s^{-|S_i|} e^{\frac{E_i - \mu_i Q_i}{T}} \pm 1\right]^{-1} \text{BW}(m_i), \tag{2.1}$$

where we include phenomenologically the strangeness saturation factor γ_s (with $|S_i|$ the total number of strange and antistrange quarks in hadron species i) to account for the possibility of incomplete equilibration in this sector; $E_i = \sqrt{p^2 + m_i^2}$ and $\text{BW}(m_i)$ is the Breit-Wigner distribution (to be replaced by a δ function for stable hadrons) to be integrated from thresholds with appropriate widths Γ_i (in practice the interval $[\max\{\text{threshold}, m_i - 2\Gamma_i\}, m_i + 2\Gamma_i]$ is sufficient). The fiducial volume V drops in particle ratios. g_i is the degeneracy factor of particle species i with vacuum mass m_i. (The study of the effect of in-medium masses (cf. [13]) is interesting because it might shed light on the chiral properties of the medium created in heavy-ion collisions at RHIC.) Eq. (2.1) simplifies in the Boltzmann approximation (i.e., discarding the spin-statistics factor ± 1) and when neglecting the energy distribution of resonances. We use here the full expression Eq. (2.1) and include all hadron states with u, d, s quarks and corresponding antiquarks up to 1.7 or 2.6 GeV [32]

TABLE I. Ratios of hadrons in Au+Au collisions at $\sqrt{s_{NN}} = 130\,\text{GeV}$ from various RHIC experiments.

Ratio	Experiment	Central	Midcentral	Peripheral
$\pi^-_{(2)} / \pi^+_{(2)}$	BRAHMS [18]	0.990 ± 0.100		
	PHENIX [19]	0.960 ± 0.177	0.920 ± 0.170	0.933 ± 0.172
	PHOBOS [21]	1.000 ± 0.022		
$\pi^-_{(1)} / \pi^+_{(1)}$	STAR [22]	1.000 ± 0.073	1.000 ± 0.073	1.000 ± 0.073
$K^+_{(2)} / K^-_{(2)}$	PHENIX [19]	1.152 ± 0.240	1.293 ± 0.268	1.322 ± 0.284
	PHOBOS [21]	1.099 ± 0.111		
	STAR [23]	1.109 ± 0.022	1.105 ± 0.036	1.120 ± 0.040
$\bar{K}^{*0} / K^{*0}$	STAR [24]	0.920 ± 0.140		
$\bar{p}_{(1)} / p_{(1)}$	PHENIX [19,20]	0.680 ± 0.149	0.671 ± 0.142	0.717 ± 0.157
$\bar{p}_{(2)} / p_{(2)}$	BRAHMS [18]	0.650 ± 0.092		
	PHOBOS [21]	0.600 ± 0.072		
	STAR [25,26]	0.714 ± 0.050	0.724 ± 0.050	0.764 ± 0.053
$\bar{\Lambda}_{(1)} / \Lambda_{(1)}$	STAR [27]	0.719 ± 0.090	0.739 ± 0.092	0.744 ± 0.100
$\bar{\Lambda}_{(2)} / \Lambda_{(2)}$	PHENIX [20]	0.750 ± 0.180	0.798 ± 0.197	0.795 ± 0.197
$\bar{\Xi}^+_{(1)} / \Xi^-_{(1)}$	STAR [28]	0.840 ± 0.053	0.822 ± 0.114	0.815 ± 0.096
$\bar{\Omega}^+ / \Omega^-$	STAR [28,29]	0.950 ± 0.158		
$K^-_{(2)} / \pi^-_{(2)}$	PHENIX [19]	0.151 ± 0.030	0.134 ± 0.027	0.116 ± 0.023
$K^-_{(2)} / \pi^-_{(1)}$	STAR [22,23]	0.151 ± 0.022	0.147 ± 0.022	0.130 ± 0.019
$K^0_s / \pi^-_{(1)}$	STAR [22,23]	0.134 ± 0.022	0.131 ± 0.022	0.108 ± 0.018
$\bar{p}_{(1)} / \pi^-_{(2)}$	PHENIX [19,20]	0.049 ± 0.010	0.047 ± 0.010	0.045 ± 0.009
$\bar{p}_{(2)} / \pi^-_{(1)}$	STAR [22,26]	0.069 ± 0.019	0.067 ± 0.019	0.067 ± 0.019
$\Lambda_{(1)} / \pi^-_{(1)}$	STAR [22,27]	0.043 ± 0.008	0.043 ± 0.008	0.039 ± 0.007
$\Lambda_{(2)} / \pi^-_{(2)}$	PHENIX [19,20]	0.072 ± 0.017	0.068 ± 0.016	0.074 ± 0.017
$\langle K^*0 \rangle / \pi^-_{(1)}$	STAR [22,24]	0.039 ± 0.011		
$\phi / \pi^-_{(1)}$	STAR [22,30]	0.022 ± 0.003	0.021 ± 0.004	0.022 ± 0.004
$\Xi^-_{(1)} / \pi^-_{(1)}$	STAR [22,28]	0.0093 ± 0.0012	0.0072 ± 0.0011	0.0060 ± 0.0008
$(\Omega^- + \bar{\Omega}^+) / \pi^-_{(1)}$	STAR [22,28]	0.0023 ± 0.0006		

with masses and total widths according to the particle data group listing [14]. The final particle numbers to be compared with experiment are $N_i = N_i^{\text{prim}} + \sum_j \text{Br}^{j\to i} N_j^{\text{prim}}$ because of decays of unstable particles with branching ratios $\text{Br}^{j\to i}$.

Originally, such a description was thought to be justified for multiplicities measured over the entire phase space, because many dynamical effects cancel out in ratios of hadron yields [5]. At sufficiently high energy, such as at RHIC, however, ratios of midrapidity yields are also found to be well described by the statistical-thermal model [1,3,12,15,16].

III. THE DATA

In contrast to SPS energies, where both midrapidity and fully phase-space-integrated data are at our disposal (see Refs. [12] for a comparison), at RHIC energy of $\sqrt{s_{NN}} = 130\,\text{GeV}$ sufficiently many data of identified hadrons are available only at midrapidity. As pointed out in Ref. [5,17] and in the first reference of Ref. [6] [cf. Eq. (5) there], the use of midrapidity data at RHIC is actually the proper procedure. The data analyzed here were compiled from PHENIX, PHOBOS, BRAHMS, and STAR experimental results. These experiments differ in their cuts on the data. It turns out that the results for the deduced thermal freeze-out parameters depend in some cases sensitively on the employed data sets. Therefore, for definiteness Table I lists the ratios used as a function of collision centrality after recalculation to a common centrality binning as in [15]. A subscript of (1) denotes yields corrected for weak feed-down, whereas yields labeled with (2) include a contribution from weak decays. Three centrality bins were selected with participant numbers 63.5 ± 8.4 (peripheral), 210.5 ± 8.4 (midcentral), and 317.0 ± 8.2 (central).

IV. THE FIT PROCEDURES

According to our propositions, T, μ_B, μ_S, and γ_s are unconstrained fit parameters. For each centrality class, four fits were performed:

Fit I: all available ratios listed in Table I included
Fit II: only ratios of π, K, p, Λ, and Ξ included
Fit III: only ratios of π, K, p, and Λ included
Fit IV: only ratios of π, K, and p included.

In this way, the effect of the various multiplicities on the thermal parameters are investigated. (Various other fitting procedures are considered in Ref. [15].)

The final ratios compared with experiment include both a primordial and a decay contribution. As mentioned above, in some cases the experimental data have been corrected for weak decays. However, where such corrections have not been made, the influence of weak decays is included in the following way:

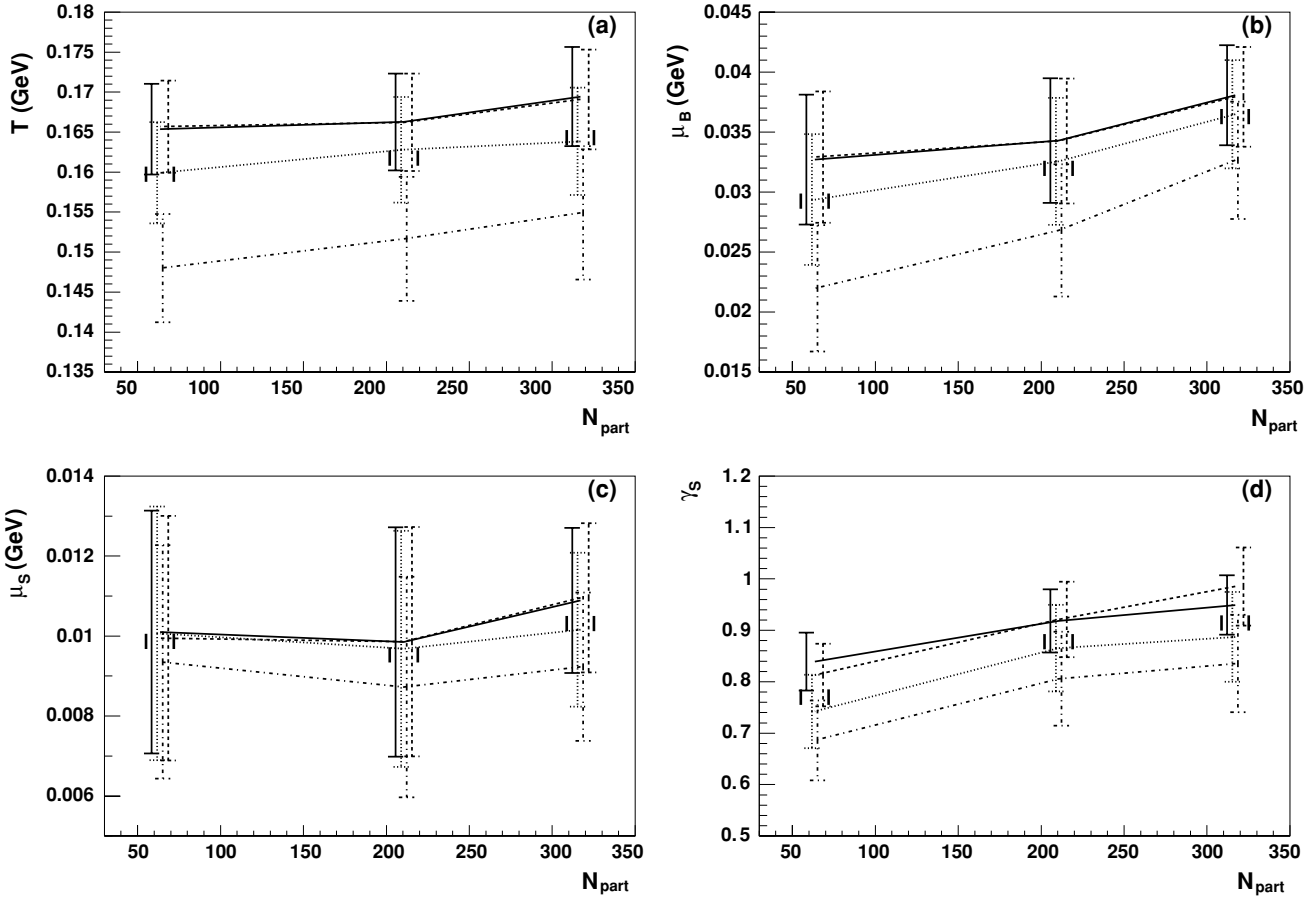

FIG. 1. The thermal parameters [(a) temperature T, (b) baryon chemical potential μ_B, (c) strangeness chemical potential μ_S, (d) strangeness saturation factor γ_s] as extracted from the experimental data for the various fit types (Fit I: solid, Fit II: dashed, Fit III: dotted, Fit IV: dash-dotted curves). To make the error bars on the parameters distinguishable, they are displaced within the corresponding $N_{\rm part}$ bins marked separately.

$\pi^{\pm}_{(2)}$: includes 50% of pions from decays of Ω, Ξ, Σ, Λ and their antiparticles as well as K^0_s
$K^{\pm}_{(2)}$: includes 100% of kaons from ϕ decay and 50% of kaons from Ω and $\bar{\Omega}$ decay
K^0_s: includes 100% of K^0_s from ϕ decay
$p_{(2)}$ and $\bar{p}_{(2)}$: includes 100% of protons from the decay of Λ, Σ^0 and their antiparticles
$\Lambda_{(2)}$ and $\bar{\Lambda}_{(2)}$: includes 100% of the contribution from the decay of Ξ, Ω and their antiparticles.

As seen in Table I, in some cases the same ratios are at our disposal from various experiments. We include these multiply given ratios in our analysis as separate data points to be fit.

V. RESULTS

A. Centrality dependence of thermal parameters

The global results of the fits are displayed in Fig. 1. As is evident from Fig. 1a, the chemical freeze-out temperature is roughly constant at around 165 MeV in Fit I. Although the strangeness chemical potential is fairly flat at $\mu_S \approx 10$ MeV [with 10% variation, Fig. 1(c)], the baryon chemical potential [Fig. 1(b)] increases slightly with participant number in the range 32.7 to 38.1 MeV (a 14% increase) in Fit I. Most striking, however, and the main result of our analysis, is the systematic increase in strangeness saturation [Fig. 1(d)] with increasing centrality for all fit types. The difference in γ_s for central and peripheral collisions is near the 1σ level; the position of the intermediate point strongly supports the trend. This confirms previous arguing [12,15]. On a quantitative level, an analysis based on too few hadron species delivers nonreliable results, in particular also for γ_s [see Fig. 1(d), Fit IV]. Fits I and II, in contrast, deliver consistent results. Because we consider the phenomenologically introduced parameter γ_s as one possible indicator of deviations from equilibrium, the conclusion is that in central collisions equilibrium conditions for describing the chemical freeze-out are appropriate, whereas more peripheral collisions point to some off-equilibrium effects.

To highlight the role of the parameter γ_s on the quality of the data fits, we exhibit in Fig. 2 the χ^2 contours for fixed values of γ_s in the $T - \mu$ plane. For definiteness, only results for Fit I and peripheral collisions are shown. We have selected $\gamma_s = 1$ (representing the assumption of full equilibrium), 0.836 (the optimum choice), and 0.5 (as rather extreme choice to evidence general trends), respectively. The corresponding χ^2/DOF

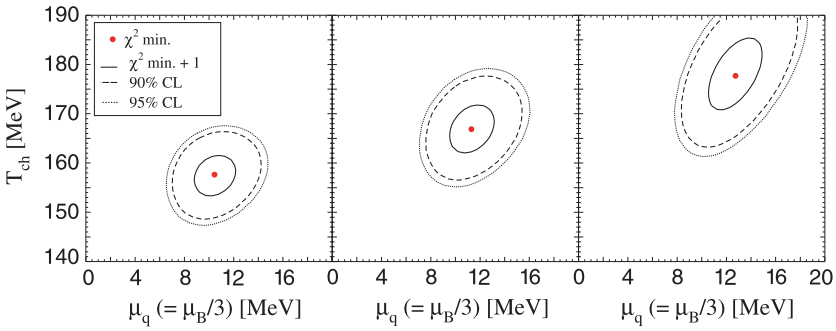

FIG. 2. (Color online) χ^2 contours from Fit I of peripheral data. $\gamma_s = 1$ (0.5) in left (right) panel. In the middle panel, $\gamma_s = 0.836$ being the optimum choice.

are 24.5/14, 16.2/13, and 59.2/14. The figure evidences that lowering γ_s noticeably shifts T up, whereas the up-shift of μ_B is less pronounced. The change in χ^2/DOF quantifies the relevance of the parameter γ_s for the fits. The large value of χ^2/DOF for $\gamma_s = 0.5$ shows the inadequacy of the model for such a parameter.

B. Detailed comparison with data

After discussing the global trends, it is worthwhile to look into details. Instead of displaying the usual comparison of model results with data in one plot we consider each ratio individually to exhibit the centrality systematics.

1. Particle/antiparticle ratios

Figure 3 summarizes such a comparison for the three centrality classes for the antiparticle/particle ratios. The data used from Table I are shown together with our model results.

For a qualitative understanding one can use the Boltzmann approximation ignoring widths. (At RHIC energies the use of Boltzmann statistics introduces errors in primordial yields at the level of 10% for pions, 1.3–1.5% for kaons and less than 1% for all other hadrons. Thus, given the intrinsic systematic uncertainties inherent in any thermal model analysis owing to the poorly constrained particle properties of the heavy resonances, quantum statistics is important only for pions.) The primordial density of hadron species i is then given by the following:

$$n_i = \frac{g_i}{(2\pi^2)} \gamma_S^{|S_i|} m_i^2 T K_2(m_i/T) \exp(\mu_i/T). \tag{5.1}$$

Thus, the ratio of particle to antiparticle primordial yields is simply,

$$\frac{n_i}{n_{\bar{i}}} = \exp(2\mu_i/T). \tag{5.2}$$

Antiparticle/particle ratios therefore fix $\mu_{B,S}/T$. We note that these ratios are only slightly affected by feed-down (using the central Fit I best-fit parameters the percentage influence of feed-down is as follows: $\pi^-_{(1)}/\pi^+_{(1)}$: 0.01%, $\pi^-_{(2)}/\pi^+_{(2)}$: 0.9%, $K^+_{(2)}/K^-_{(2)}$: 2.8%, $\bar{K}^{*0}/K^{*0}$: 0.4%, $\bar{p}_{(1)}/p_{(1)}$: 0.5%, $\bar{p}_{(2)}/p_{(2)}$: 3.5%, $\bar{\Lambda}_{(1)}/\Lambda_{(1)}$: 0.7%, $\bar{\Lambda}_{(2)}/\Lambda_{(2)}$: 4.0%, $\bar{\Xi}^+_{(1)}/\Xi^-_{(1)}$: 0.02%, and $\bar{\Omega}/\Omega$: 0%). Thus, the trends in these ratios translate directly into trends in μ_S/T and μ_B/T, whereas they are roughly insensitive to γ_S and T.

Let us now consider the individual ratios and begin with π^-/π^+. The experimental ratio is consistent with being flat and slightly below or equal to unity. Our model yields a $\pi^-_{(2)}/\pi^+_{(2)}$ ratio slightly above 1 [see Fig. 3(a)] and a $\pi^-_{(1)}/\pi^+_{(1)}$ ratio slightly below 1 [see Fig. 3(b)]. Model and experiment, however, agree within errors. There is no significant difference between the results of the four fits. Setting $\mu_Q = 0$ drives the model ratio to very close to 1; deviations are because of feeding (because μ_B and μ_S are both greater than zero). With only strong decays included, the ratio is less than 1. Therefore it is the influence of the weak decays that pushes the ratio $\pi^-_{(2)}/\pi^+_{(2)}$ above 1. This ratio is insensitive to μ_S and μ_B: with a 5-MeV change in μ_B the ratio varies by 0.2%, whereas a 5-MeV change in μ_S leads to a 0.3% change in the ratio. A 0.2 change in γ_S furthermore affects the ratio by only 0.2%, whereas a 5-MeV change in T leads to only a 0.06% change in the ratio. $\pi^-_{(1)}/\pi^+_{(1)}$ is even less sensitive to variations in T, μ_B, μ_S, and γ_S. Therefore, the ratio π^-/π^+ fixes nothing and serves just as the motivation for setting $\mu_Q = 0$.

The ratio $K^+_{(2)}/K^-_{(2)}$ is above 1 [see Fig. 3(c)] and drives μ_S to positive values. Because of their much smaller errors, the STAR ratios are heavily weighted in the fit. This contributes to μ_S having a slight kink as seen in Fig. 1(c). The effect of the above-quoted feeding accounts for the slightly different shape of the K^+/K^- ratio compared with the μ_S/T trend that can be deduced from Fig. 1. With this ratio removed from the fit, μ_S/T would increase steeply with centrality, driven by the $\bar{\Lambda}/\Lambda$ to $\bar{\Xi}^+/\Xi^-$ double ratio. This gives $\bar{\Xi}^+/\Xi^-$ an increasing trend. To keep the $\bar{\Lambda}/\Lambda$ ratio flat, μ_B/T then similarly increases which causes $\bar{p}/p$ to drop. Therefore, the kaon ratio is what keeps μ_S flattish and gives it the "kink".

The $\bar{p}/p$ experimental ratios differ noticeably [see Figs. 3(e) and 3(f)], with STAR being the highest. These STAR data points are favored in fits because they have much reduced errors (consistently a factor of 3 less than those of PHENIX). These STAR ratios, however, are too high if the STAR $\bar{\Lambda}/\Lambda$ ratio is to be simultaneously reproduced by the model (STAR $\bar{p}/p$ supports a lower μ_B as is seen when the Λs are removed from the fit, as done in Fit IV). With Λs excluded, the much smaller STAR errors lead to these $\bar{p}/p$ data points being strongly favored in the midcentral and peripheral fits. This leads to a strong increase of μ_B with centrality. Because the experimental $\bar{\Lambda}/\Lambda$ ratio [Figs. 3(g) and 3(h)] is flattish, they support a similar behavior for μ_B/T and μ_S/T.

Excluding all but the STAR $\bar{p}/p$ points in the most central bin removes the strong increase in μ_B from the midcentral to central bins seen in Fit IV. Our suspicion that it is $\bar{p}/p$ that causes μ_B to increase is confirmed by repeating the fits with

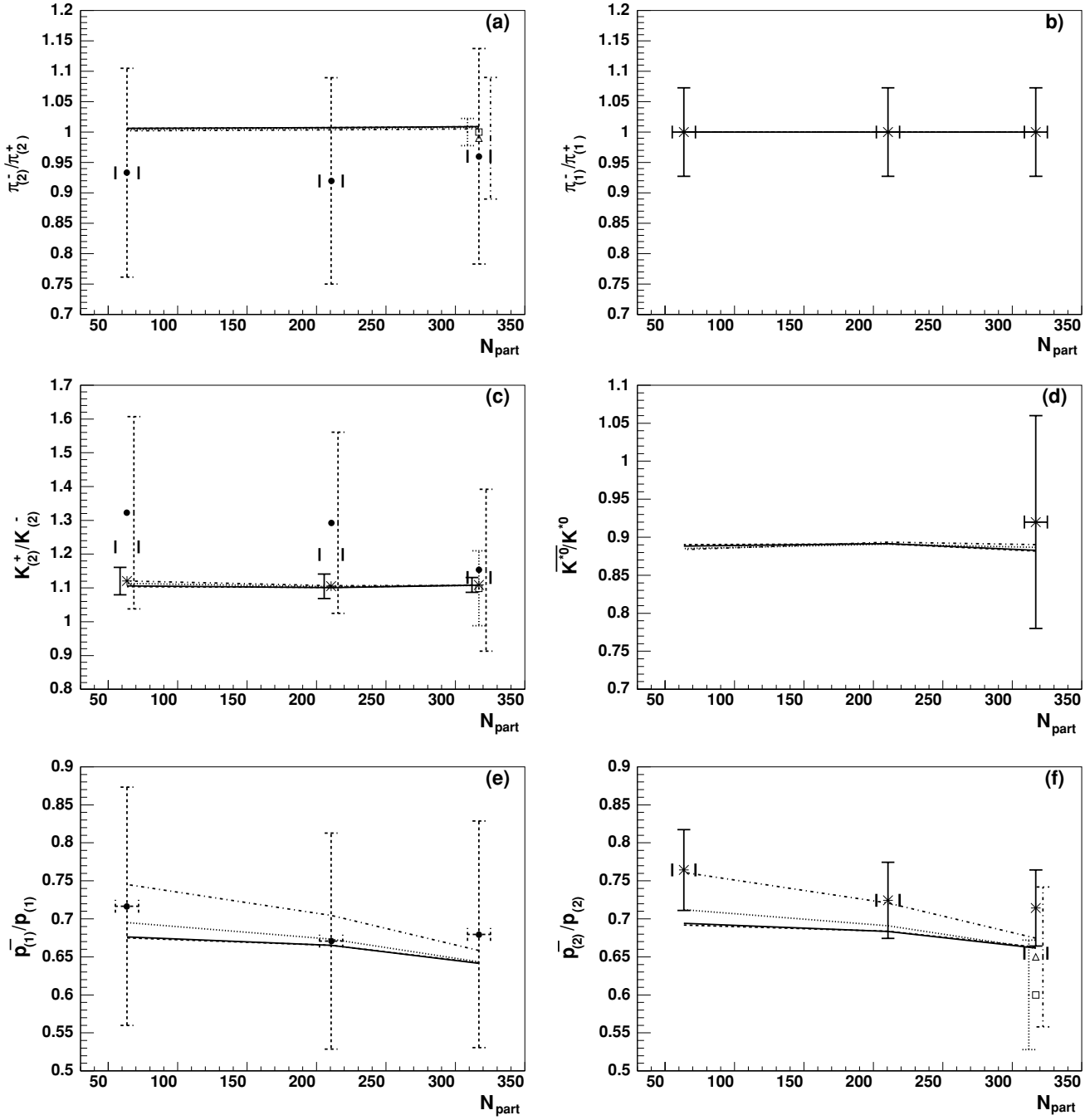

FIG. 3. Comparison between experiment (error bars displaced within $N_{\rm part}$ bins whenever necessary to make them distinguishable) and model results for particle/antiparticle ratios [(a) $\pi^-_{(2)}/\pi^+_{(2)}$, (b) $\pi^-_{(1)}/\pi^+_{(1)}$, (c) $K^+_{(2)}/K^-_{(2)}$, (d) $\bar{K}^{*0}/K^{*0}$, (e) $\bar{p}_{(1)}/p_{(1)}$, (f) $\bar{p}_{(2)}/p_{(2)}$]. Line codes as described in the legend to Fig. 1, experimental results: STAR: stars (solid error bars), PHENIX: circles (dashed error bars), PHOBOS: squares (dotted error bars), BRAHMS: triangles (dash-dotted error bars), cf. Table I.

only antiparticle/particle ratios included (i.e., all particle/pion ratios excluded). Because these ratios are insensitive to γ_S, and T enters only together with the chemical potentials, in these reduced fits we fixed $\gamma_S = 1$ and $T = 165$ MeV (both reasonable in light of the full results). The approximate trends in μ_S/T and μ_B/T observed in the full fits were reproduced using just these ratios. With the $\bar{p}/p$ ratio excluded, the steady increase in μ_B disappears; instead μ_B/T decreases similarly to μ_S/T as driven by the flatness in the $\bar{\Lambda}/\Lambda$ ratio.

The ratio $\bar{\Xi}^+/\Xi^-$ [see Fig. 3(i)] depends strongly on μ_S/T and μ_B/T and is little affected by feed-down. Similar fractional errors to the corrected $\bar{\Lambda}/\Lambda$ ratio means both are treated equally in fits. Although consistent within errors, the model trend decreases slightly with centrality, whereas the

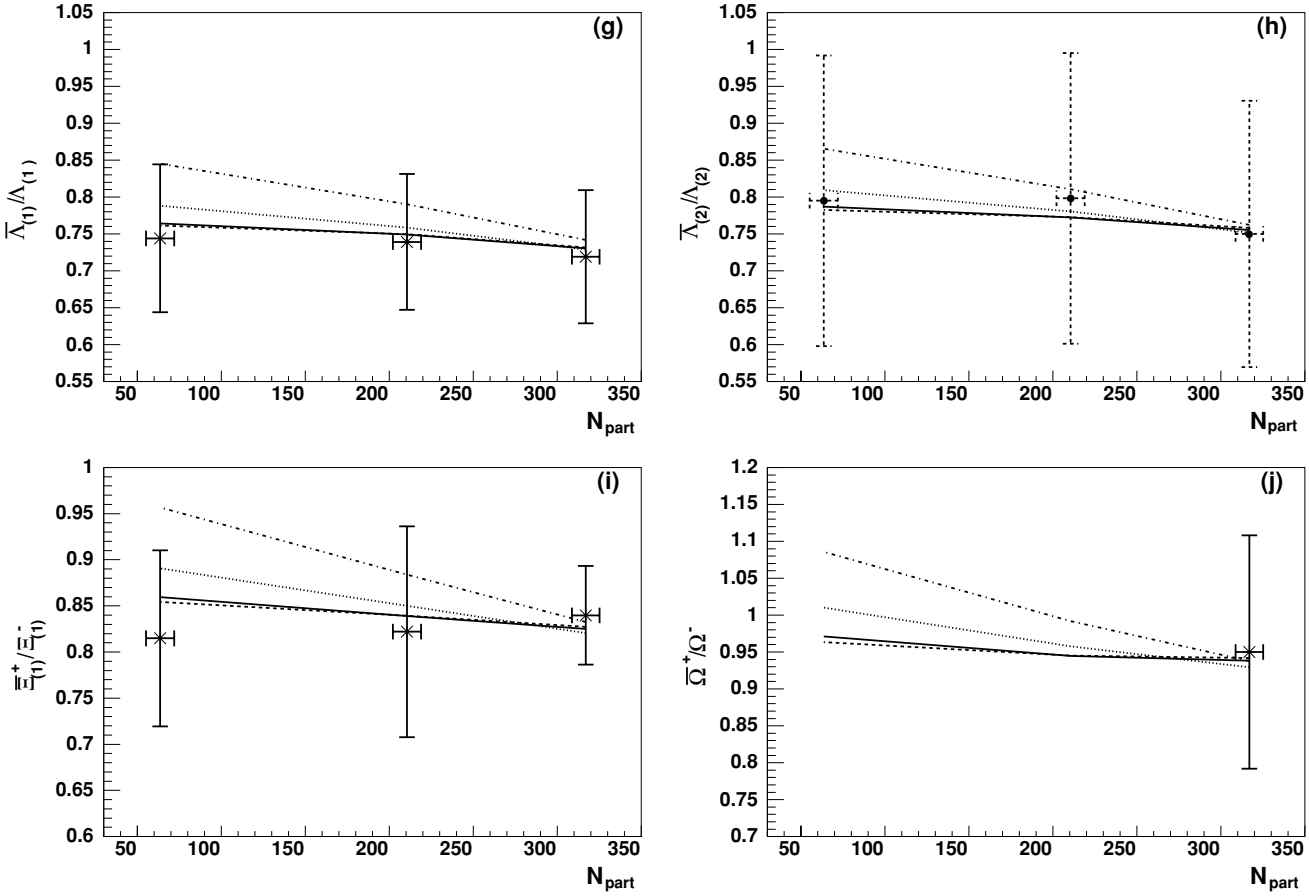

FIG. 3. *(Continued.)* (g) $\bar{\Lambda}_{(1)}/\Lambda_{(1)}$, (h) $\bar{\Lambda}_{(2)}/\Lambda_{(2)}$, (i) $\bar{\Xi}^{+}_{(1)}/\Xi^{-}_{(1)}$, (j) $\bar{\Omega}^{+}/\Omega^{-}$.

data are consistent with a weak increase. Comparing this experimental ratio with $\bar{\Lambda}/\Lambda$, the $\bar{\Xi}^{+}/\Xi^{-}$-to-$\bar{\Lambda}/\Lambda$ double ratio increases. Thus, μ_S/T is driven up particularly from the midcentral to central bin. As mentioned, the K^{+}/K^{-} ratio leads to a kink in the trend for μ_S. This effect wins over the influence of the $\Xi\Lambda$ double ratio, which suggests an increase in μ_S/T.

Unfortunately there is no centrality information on the ratios $\bar{\Omega}^{+}/\Omega^{-}$ or $\bar{K}^{0*}/K^{0*}$. Such data would allow even better determination of μ_S. As seen in Figs. 3(d) and 3(j), our model results agree fairly well with the data for the central bin.

2. Particle/pion ratios

The particle/pion ratios read in the Boltzmann approximation, neglecting width and quantum statistics for a tentative consideration of generic features as follows:

$$\frac{n_i}{n_\pi} = \gamma_S^{|S_i|}\frac{g_i}{g_\pi}\frac{m_i^2}{m_\pi^2}\frac{K_2(m_i/T)}{K_2(m_\pi/T)}\frac{\exp(\mu_i/T)}{\exp(\mu_\pi/T)}, \tag{5.3}$$

that is, qualitatively, mixed particle ratios allow the determination of γ_S and T and hence the μs independently. Whereas the particle/antiparticle ratios feature just the combination μ/T, the primordial particle/pion ratios also feature T in the combination $K_2(m_i/T)/K_2(m_\pi/T)$. This allows the temperature to be fixed and then, given the values of μ/T fixed by the particle/antiparticle ratios, the chemical potentials are determined. However, feed-down plays an important role in these ratios, so that the final observed ratios differ from the ratios of primordial densities quite substantially. This makes a detailed analysis of the influence of these ratios on the parameters much more difficult than in the case of the particle/antiparticle ratios. In fact, for the best-fit parameters corresponding to Fit I of the central bin, more than 70% of π^{+}s come from decays.

A simple analysis shows how the ratio $K_2(m_i/T)/K_2(m_\pi/T)$ varies with temperature for a number of hadron species i: Lowering the temperature has the effect of bringing the particle/pion ratios down. Furthermore, the fractional effect of changing the temperature is greater for the heavier particles.

After these general remarks let us consider in some detail the comparison of our model with data. We use, of course, again full quantum statistics. The ratios $K^{-}_{(2)}/\pi^{-}_{(2)}$ [Fig. 4(a)] and $K^{-}_{(2)}/\pi^{-}_{(1)}$ [Fig. 4(b)] are reasonably well reproduced in the fits. Because the errors on the PHENIX and STAR experimental ratios are similar, neither is heavily biased in the fit. The PHENIX data rise more rapidly than the STAR data (especially from the midcentral to central bin). Because

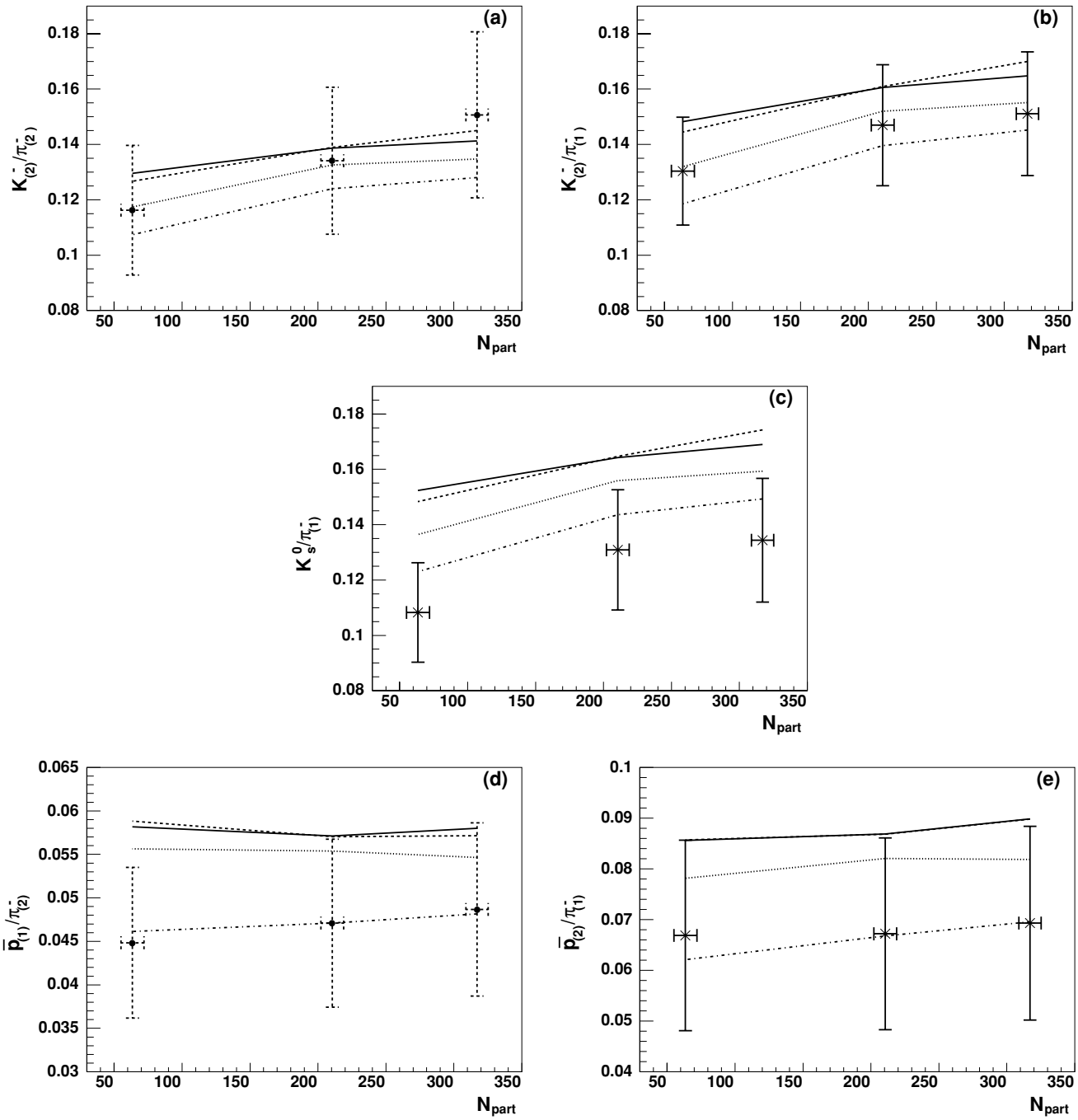

FIG. 4. As in Fig. 3 but for particle/pion ratios [(a) $K^-_{(2)}/\pi^-_{(2)}$, (b) $K^-_{(2)}/\pi^-_{(1)}$, (c) $K^0_s/\pi^-_{(1)}$, (d) $\bar{p}_{(1)}/\pi^-_{(2)}$, (e) $\bar{p}_{(2)}/\pi^-_{(1)}$].

the particle/antiparticle ratios support a centrality-independent μ_S/T, the experimental K^-/π^- ratios drive an increase in strangeness saturation, with the PHENIX data supporting a steeper increase in γ_S than the data [see Fig. 1(d)]. In Fit I and II K^-/π^- is overpredicted with the exception of the central $K^-_{(2)}/\pi^-_{(2)}$ data point. In contrast, the uncorrected Λ/π^- and Ξ^-/π^- are underestimated (small fractional errors on Ξ^-/π^- mean that this ratio strongly influences the fit). With the Ξs removed in Fit III the STAR K^-/π^- data are well reproduced owing to the drop in T and γ_S. The big drop in this ratio when Λs are excluded from the fit is because of the further drop in γ_S and T in Fit IV seen in Fig. 1. The effect of this drop is somewhat lessened by the accompanying drop in μ_S/T in the central and midcentral bins. Furthermore, the kaonpion ratios are least affected by the temperature change in Fit IV.

The increase in the ratio K^0_S/π^- with centrality [Fig. 4(c)] also drives γ_S to increase. In the full fits (Fits I–III) it is somewhat overestimated (a similar result is found in Ref. [15]),

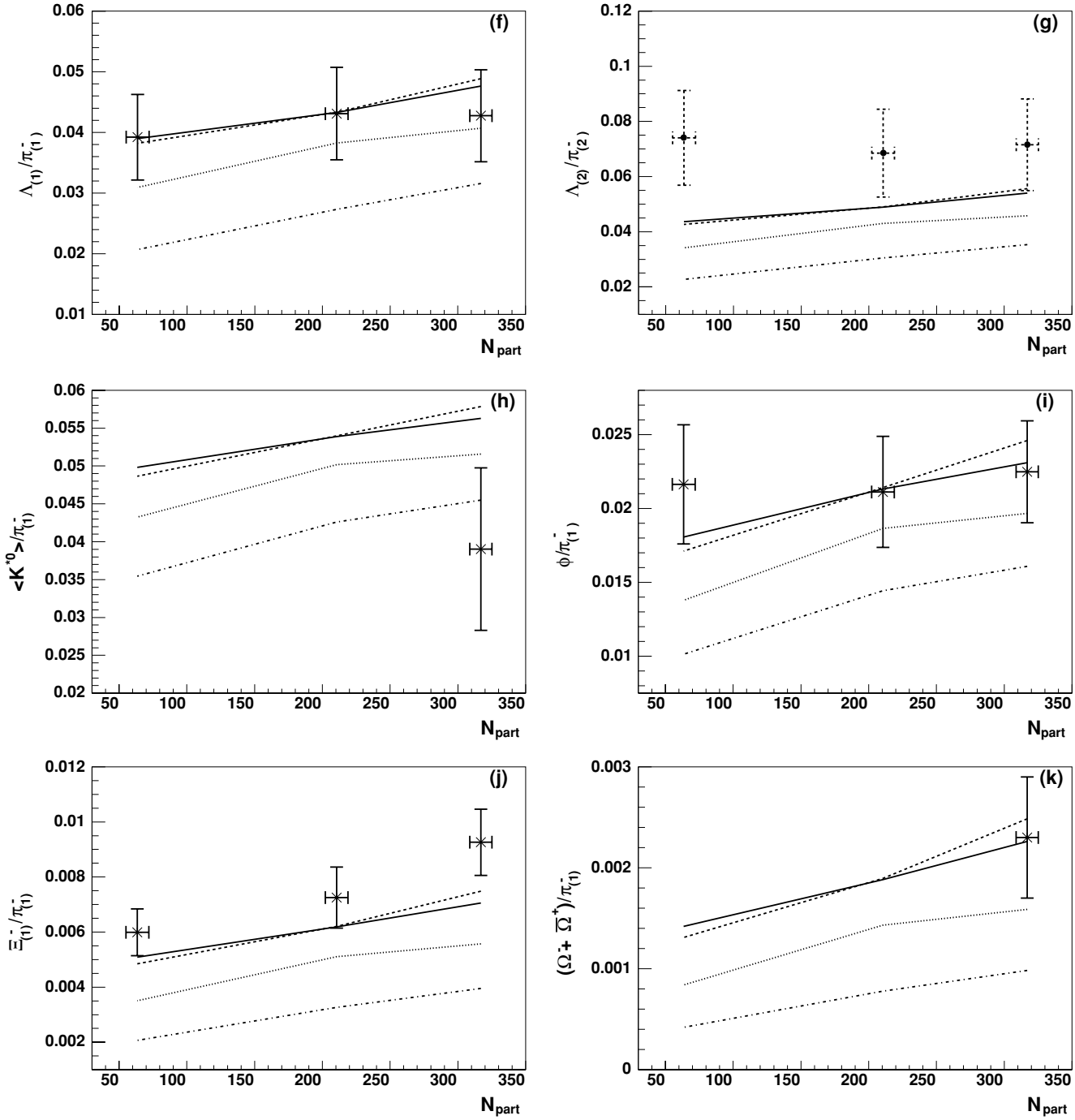

FIG. 4. *(Continued.)* (f) $\Lambda_{(1)}/\pi^-_{(1)}$, (g) $\Lambda_{(2)}/\pi^-_{(2)}$, (h) $\langle K^{*0}\rangle/\pi^-_{(1)}$, (i) $\phi/\pi^-_{(1)}$, (j) $\Xi^-_{(1)}/\pi^-_{(1)}$, (k) $(\Omega^- + \bar{\Omega}^+)/\pi^-_{(1)}$.

whereas the exclusion of the Λ's (Fit IV) results in much better agreement. This is owing to the reduced γ_S in Fit IV. The central $\langle K^{*0}\rangle/\pi^-$ ratio reproduction by the model [Fig. 4(h)] follows the same trend as the K^0_S.

Let us now focus on the $\bar{p}/\pi^-$ and Λ/π^- ratios [Figs. 4(d), 4(e), 4(f) and 4(g)]. Although the $\bar{p}/\pi^-$ ratio is overestimated by the model in Fits I–III, Λ/π^- is underestimated except for the corrected Λ/π^- in the central and midcentral bins in Fits I and II. With Λ excluded, $\bar{p}/\pi^-$ is well reproduced, whereas Λ/π^- is greatly underpredicted. Therefore, $\bar{p}/\pi^-$ drives T down, whereas Λ/π^- tends to raise γ_S and T.

The flatness of the ratio ϕ/π^- [Fig. 4(i)] supports a centrality-independent γ_S. In Fits I and II there is fair agreement with the model, whereas this ratio is greatly underestimated in Fit IV owing to the greatly reduced γ_S and T. The increasing trend of the model results is because

of the increase in γ_S with centrality and the fact that $n_\phi \sim \gamma_S^2$.

The increase of the ratio Ξ^-/π^- [Fig. 4(j)] drives μ_B/T to increase as well as γ_S. Conversely, it causes μ_S/T to drop. Again there is fair agreement with the model in Fits I and II, whereas this ratio is greatly underestimated in Fit IV.

There is fair agreement of our model results with the $(\Omega^- + \bar{\Omega}^+)/\pi^-$ ratio [Fig. 4(k)] in the central bin in Fits I and II. However, with Ξ and Λ removed agreement worsens.

Our final conclusion is that Fits I–II give a quite satisfactory description of most ratios, with the exception of K_S^0/π^-, $\langle K^{*0}\rangle/\pi^-$, and corrected $\bar{p}/\pi^-$. For the $\langle K^{*0}\rangle/\pi^-$ and $(\Omega^- + \bar{\Omega}^+)/\pi^-$ there are no data for midcentral and peripheral collisions. Thus our results may serve as predictions.

C. Summary

In summary, we present an analysis of the centrality dependence of thermal parameters deduced from hadron multiplicities within a statistical-thermal model. The grand-canonical formalism is employed with quantum statistics and resonance widths included for all of the fits. We rely entirely on published data for the reaction Au+Au at $\sqrt{s_{NN}} = 130\,\text{GeV}$. Our aim is to employ the strangeness saturation factor γ_s as one possible indicator for deviations from equilibrium conditions in describing the chemical freeze-out. Indeed, for noncentral collisions the systematic deviation of γ_s from unity can be considered as a hint to off-equilibrium effects, whereas for central collisions and using a sufficiently complete set of available multiplicity ratios at midrapidity there is no indication for deviations from equilibrium conditions.

We present a detailed comparison of the model results with data. The trends in $\mu_{B,S}/T$ are fixed by the antiparticle/particle ratios. The K^+/K^- ratio is responsible for keeping μ_S/T essentially flat. This wins over the influence of the Ξ to Λ double ratio, which tends to increase μ_S/T. The $\bar{p}/p$ ratio drives μ_B/T up, which wins over $\bar{\Lambda}/\Lambda$s attempts to make μ_S/T and μ_B/T behave similarly. The temperature and strangeness saturation are fixed by the particle/pion ratios. The observed increase in γ_S is driven predominantly by the increase in the K^-/π^- ratio and the flatness of μ_S/T as fixed by the K^+/K^- ratio.

A possible extension of the present work is the analysis of saturation in the nonstrange sector, parameterized by γ_q being a factor similar to γ_s [31]. Because our fits to the data deliver reasonably small values of χ^2 we believe, however, that there is not too much room left for sizeable deviations of γ_q from unity. This issue deserves a separate investigation. More tempting is the analysis of data for $\sqrt{s_{NN}} = 200\,\text{GeV}$. The explorative study in Ref. [15] points to a similar behavior of γ_s as we find for $\sqrt{s_{NN}} = 130\,\text{GeV}$. Even more interesting is to test heavy flavor production; because of their larger intrinsic masses, heavy flavors should have a higher sensitivity to the medium. In particular, hadrons with open and hidden charm may require a corresponding factor γ_c.

ACKNOWLEDGMENTS

This work has been supported in part by the National Research Foundation of South Africa, the U.S. Department of Energy under contract no. DE-AC03-76SF00098 and the German BMBF grant 06DR121.

[1] P. Braun-Munzinger, K. Redlich, and J. Stachel, nucl-th/0304013, in *Quark-Gluon Plasma 3*, edited by R. Hwa and X. N. Wang, p. 491; K. Redlich, J. Cleymans, H. Oeschler, and A. Tounsi, Acta Phys. Polonica B **33**, 1609 (2002); J. Letessier and J. Rafelski, Int. J. Mod. Phys. E **9**, 107 (2000).

[2] F. Becattini, J. Cleymans, A. Keränen, E. Suhonen, and K. Redlich, Phys. Rev. C **64**, 024901 (2001).

[3] P. Braun-Munzinger *et al*., Phys. Lett. **B344**, 43 (1995); **B365**, 1 (1996); **B465**, 15 (1999); **B518**, 41 (2001).

[4] J. Cleymans and K. Redlich, Phys. Rev. Lett. **81**, 5284 (1998); J. Sollfrank, J. Phys. G: Nucl. Part. Phys. **23**, 1903 (1997).

[5] J. Cleymans, K. Redlich, Phys. Rev. C **60**, 054908 (1999).

[6] W. Broniowski and W. Florkowski, Phys. Rev. C **65**, 064905 (2002); Phys. Rev. Lett. **87**, 272302 (2001); F. Becattini and G. Passaleva, Eur. Phys. J. C **23**, 551 (2002)

[7] P. Braun-Munzinger, J. Stachel, and C. Wetterich, Phys. Lett. **B596**, 61 (2004).

[8] T. Biro, B. Müller, Phys. Lett. **B578**, 78 (2004); A. Majumder and V. Koch, Phys. Rev. C **68**, 044903 (2003).

[9] P. Koch, B. Müller, and J. Rafelski, Phys. Rep. **142**, 167 (1986); J. Letessier, J. Rafelski, and A. Tounsi, Phys. Rev. C 50, **406** (1994); C. Slotta, J. Sollfrank, and U. Heinz, AIP Conf. Proc. (Woodbury) **340**, 462 (1955).

[10] F. Becattini, M. Gazdzicki, A. Keränen, J. Manninen, and R. Stock, Phys. Rev. C **69**, 024905 (2004); I. G. Bearden *et al*. (NA44 Collaboration), *ibid.* **66**, 044907 (2002); F. Becattini, M. Gazdzicki, and J. Sollfrank, Eur. Phys. J. C **5**, 143 (1998).

[11] J. Cleymans, B. Kämpfer, and S. Wheaton, Phys. Rev. C **65**, 027901 (2002).

[12] J. Cleymans, B. Kämpfer, and S. Wheaton, Nucl. Phys. **A715**, 553c (2003); J. Cleymans, B. Kämpfer, P. Steinberg, and S. Wheaton, hep-ph/0212335, J. Phys. G **30**, S595 (2004); B. Kämpfer, J. Cleymans, K. Gallmeister, and S. Wheaton, hep-ph/0202134, Acta. Phys. Hung. New Ser. Heavy Ion Phys. **18**, 1 (2003).

[13] D. Zschiesche, S. Schramm, J. Schaffner-Bielich, H. Stöcker, and W. Greiner, Phys. Lett. **B552**, 7 (2002).

[14] K. Hagiwara *et al*., Particle Data Group. Phys. Rev. D **66**, 010001 (2002).

[15] M. Kaneta, N. Xu, nucl-th/0405068.

[16] F. Becattini, J. Phys. G **28**, 1553 (2002); D. Magestro, *ibid.* **28**, 1745 (2002); A. Baran, W. Broniowski, and W. Florkowski, Acta Phys. Pol. B **35**, 779 (2004).

[17] J. Cleymans, Talk presented at "Physics and Astrophysics of the Quark-Gluon Plasma." (ICPAQGP 97), Jaipur, India,

17–21 March 1997, edited by B. C. Sinha, D. K. Srivastava, and Y. P. Viyogi, (Narosa Publishing House, 1998); Yu. M. Sinyukov, S. V. Akkelin, and A. Yu. Tolstykh, Nukleonik **43**, 369 (1998).

[18] C. Adler *et al.* (STAR Collaboration), Phys. Rev. Lett. **87**, 092301 (2002).

[19] K. Adcox *et al.* (PHENIX Collaboration), Phys. Rev. Lett. **88**, 242301 (2002).

[20] K. Adcox *et al.* (PHENIX Collaboration), Phys. Rev. Lett. **89**, 092302 (2002).

[21] B. B. Back *et al.* (PHOBOS Collaboration), Phys. Rev. Lett. **87**, 102301 (2001).

[22] J. Adamas *et al.* (STAR Collaboration), nucl-ex/0311017; M. Calderon de la Barca Sanchez, nucl-ex/0111004.

[23] C. Adler *et al.* (STAR Collaboration), Phys. Lett. **B595**, 143 (2004).

[24] C. Adler *et al.* (STAR Collaboration), Phys. Rev. C **66**, 061901(R) (2002).

[25] C. Adler *et al.* (STAR Collaboration), Phys. Rev. Lett. **86**, 4778 (2001).

[26] J. Adamas *et al.* (STAR Collaboration), Phys. Rev. C **70**, 041901(R) (2004).

[27] C. Adler *et al.* (STAR Collaboration), Phys. Rev. Lett. **89**, 092301 (2002).

[28] J. Adamas *et al.* (STAR Collaboration), Phys. Rev. Lett. **92**, 182301 (2004).

[29] J. Adamas *et al.* (STAR Collaboration), Phys. Lett. **B567**, 167 (2003).

[30] C. Adler *et al.* (STAR Collaboration), Phys. Rev. C **65**, 041901(R) (2002).

[31] J. Letessier and J. Rafelski, Phys. Rev. C **59**, 947 (1999).

[32] Actually we use two independent codes with different upper limits of the employed hadronic mass spectrum. The corresponding differences in results are tiny. One of the codes is described in S. Wheaton, J. Cleymans, hep-ph/0407174.